crystals

MDPI

Article

Single-Crystal Growth of Sr_2RuO_4 by the Floating-Zone Method Using an Infrared Image Furnace with Improved Halogen Lamps

Naoki Kikugawa [1,*], Dmitry A. Sokolov [2], Tohru Nagasawa [3] and Andrew P. Mackenzie [2,4]

1 National Institute for Materials Science, Ibaraki 305-0003, Japan
2 Max Plank Institute for Chemical Physics of Solids, D-01187 Dresden, Germany; Dmitry.Sokolov@cpfs.mpg.de (D.A.S.); Andy.Mackenzie@cpfs.mpg.de (A.P.M.)
3 Canon Machinery Inc., Shiga 524-0044, Japan; nagasawa.tohru@mail.canon
4 School of Physics and Astronomy, University of St. Andrews, St. Andrews KY16 9SS, UK
* Correspondence: KIKUGAWA.Naoki@nims.go.jp

Abstract: We report the single-crystal growth of the unconventional superconductor Sr_2RuO_4, on which research has reached a turning point recently. In order to optimize the quality of crystals grown by the floating-zone method using an infrared image furnace, we focus on an improvement of the structure of the filament in the halogen lamps. By reducing the thickness of the total filament, the form of the molten zone was narrowed. More importantly, the molten zone was observed to be more stable during the growth process. Finally, we obtained the crystals with a length of 12 cm. Additionally, the grown crystal has high quality, displaying the 1.5 K transition temperature expected only for the purest crystals. We also discuss the availability of the newly developed halogen lamps.

Keywords: floating-zone technique; single crystal; Sr_2RuO_4; molten-zone controlling

Citation: Kikugawa, N.; Sokolov, D.A.; Nagasawa, T.; Mackenzie, A.P. Single-Crystal Growth of Sr_2RuO_4 by the Floating-Zone Method Using an Infrared Image Furnace with Improved Halogen Lamps. *Crystals* **2021**, *11*, 392. https://doi.org/10.3390/cryst11040392

Academic Editors: Mihai-Ionut Sturza and Shiv J. Singh

Received: 18 March 2021
Accepted: 6 April 2021
Published: 8 April 2021

1. Introduction

Since the discovery of the superconductivity in the layered perovskite ruthenate Sr_2RuO_4 in 1994 [1], the material has attracted much attention because of the novel superconductivity with the transition temperature (T_c) of 1.50 K [2–4]. The normal state properties have been well established in the framework of Fermi-liquid theory on the basis of the quasi-cylindrical Fermi-surfaces revealed by de Haas–van Alphen and angle-resolved photoemission experiments [5–8]. On the other hand, full understanding of the superconducting state has still been a challenging issue, although many experimental probes have been attempted [9–12]. Since the unconventional superconductivity of this material is extremely fragile against any kinds of impurities and defects [13–16], progress in understanding the superconducting states has been closely linked with the improvement of quality of the available single crystals. The floating-zone technique has been the main source of such high-quality single-crystals because this method can minimize the accidental contamination of impurities during the growth processes [17,18].

Recent significant progress has been achieved by a sophisticated experimental technique, applying uniaxial stress to this material [19,20]. The technique, precisely controlled by piezo actuators, has enabled the application of compressive (tensile) uniaxial stress along in-plane direction up to over 1 GPa (around 0.2 GPa) [21]. The transition temperature reaches 3.5 K at a critical stress (~0.7 GPa) [22–24], at which one of the major bands (γ band) touches a van Hove point in the two-dimensional Brillouin zone [25]. The upper critical field along the in-plane direction is also enhanced to 4.5 T at the critical stress from 1.5 T under ambient pressure. The enhancement of the critical field along the perpendicular to the RuO_2 planes (c axis) is more remarkable: From 0.075 T under ambient pressure to 1.5 T at the critical uniaxial stress [22]. Very recently, new nuclear magnetic resonance (NMR) measurements have revealed that the spin susceptibility drops below T_c under ambient

pressure as well as uniaxial stress [26,27]. Since this observation suggests that the superconducting condensate has an even parity, rather than the odd parity proposed by a previous NMR study [28], research on this material has reached a turning point. Furthermore, a long range ordered magnetism has been induced under extreme strain (>1 GPa) [29] and seen to be neighboring the superconducting phase. All of this has stimulated widespread new interest in obtaining a full understanding of the unconventional superconductivity [30,31].

The experimental techniques for studying Sr_2RuO_4 vary from microscopic to macroscopic methods, from ambient pressure to applied uniaxial stress/hydrostatic pressure, and high-quality crystals have been in high demand for experiments aiming to reveal intrinsic properties. The most quality-sensitive feature noted so far is the detection of the first-ordered phase transition at 1.5 T when the magnetic field is exactly aligned to the in-plane direction. Here, an impurity level corresponding to 50 ppm (T_c = 1.45 K without strain) is enough to obscure the transition [32–34]. Additionally, the sample volume has become an additional factor as crystals are required, in particular, for muon spin rotation and neutron scattering experiments under strain, in order to gain a good enough signal to noise ratio for the experiments to be practical [35]. Obtaining larger crystals is also highly desirable, because growth of larger crystals enables comparison of the results of a variety of experiments on crystals from a single batch, and therefore an improved picture of the underlying physics of this material. In this paper, we report progress in the crystal growth in Sr_2RuO_4 with a focus on the benefits brought by improved halogen lamps in an infrared image furnace.

2. Experimental Section

2.1. Floating-Zone Technique

For the growth of single-crystalline Sr_2RuO_4, we employed a RuO_2 self-flux floating-zone technique using an infrared image furnace with double-elliptical mirrors (Canon Machinery Inc., SCI-MDH-11020) in Dresden. A sketch of the furnace is shown in Figure 1. Since a halogen lamp is set to one of the focal points of the gold-coated elliptical mirror, the radiation from the lamp reflected at the mirror condenses at the other focal point. The focused area is shared with the other condensed area from the radiation of the second lamp, and reaches over 2000 °C when both lamps are operated at maximum power. Then, the bottom end of an RuO_2-enriched feed rod attached to the upper shaft is carried to the focus. The molten rod is connected to a seed rod attached to the lower shaft, and the molten zone is formed. The single crystal finally forms as it is pulled continuously from the molten zone. The growth area is separated by a quartz tube from the outside, and we are able to choose the desirable gas and its pressure for the growth. Here, one of the important points is to keep the molten zone stable during the growth, because it is supported only by the surfaces between the feed rod and the seed rod. There are many controllable parameters to stabilize the molten zone, for example, the lamp power, the feed speed, the seed speed, the gas atmosphere, the applied pressure, and the quality of the rod, and we have succeeded in growing the Sr_2RuO_4 crystals by optimizing these parameters [17,18]. We argue that this optimization has been focused on the growth processes, not on the hardware setup of the infrared furnace.

2.2. Controlling the Molten Zone

In this paper, we focus on another parameter, the molten zone itself, which has not been paid as much attention regarding the growth of ruthenates since the early work in the second half of the 1990s. Our experience throughout the crystal growth is that the molten zone of the (layered) perovskite ruthenates has relatively low surface tension and viscosity [36–39], compared to, for instance, rutile (TiO_2) and aluminum oxide (Al_2O_3), which are the typical materials used for the test growth when the furnace is first installed. It is, therefore, usually hard to keep the molten zone stable for the growth of ruthenates. Since the liquid state of the molten zone is an intrinsic property of the material, it cannot

be controlled during the growth. Instead, one can control the shape of the molten zone by sharpening/expanding the focused area.

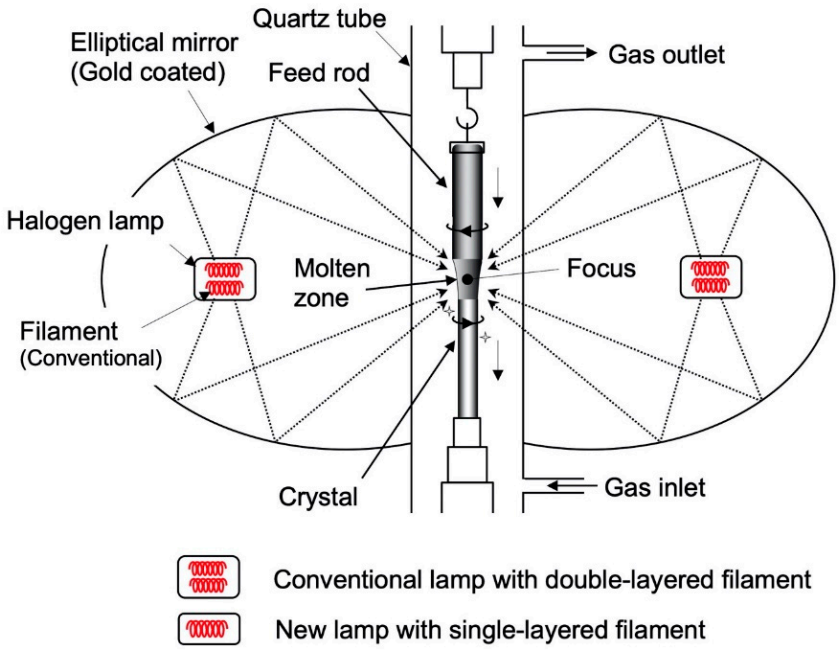

Figure 1. Schematic drawing of an infrared image furnace with double elliptical mirrors. In this study, we focus on the improvement of the crystal growth of Sr_2RuO_4 by introducing a new filament. Here, the new filament has a single layered, whereas the conventional one has a double-layered structure.

The focus area is strongly influenced by the filament dimension of the halogen lamp, as shown in Figure 2. The filament first used to attempt the growth of ruthenates had the spiral structure shown in Figure 2a, but a significant advance was made [17,36] by replacing it with a flat-shaped filament in early 1997. The flat-shaped filament used since then has a double-layered structure (Figure 2b), where each layer is formed by an array of filaments. Since the layered filament sits horizontally at the focus point of the elliptical mirror, the vertical length at the molten zone depends on the thickness of the total filament. Thus far, we have chosen the double-layered filaments with the total thickness of 6 mm in order to gain a sufficient power to melt the feed rods of ruthenates over 2000 °C. Consequently, the molten zone was broadened to typically 8 mm.

We have developed a new filament to reduce the length of the molten zone, as shown in Figure 2c. The significant point is that the new filament is formed by a single layer, rather than the double layer, and the thickness is reduced to 2 mm. We note that the same electrical power of the new single-layered filament (2 kW) is kept compared to that of the conventional double-layered filament, although the total volume of the filament is reduced by 40%. Next step is to examine the growth of Sr_2RuO_4 in order to check how the new filament improves the growth, because the narrower molten zone might actually cause a more unstable situation during the growth: The bottom of the feed rod and the top of the seed confront each other because both are getting closer.

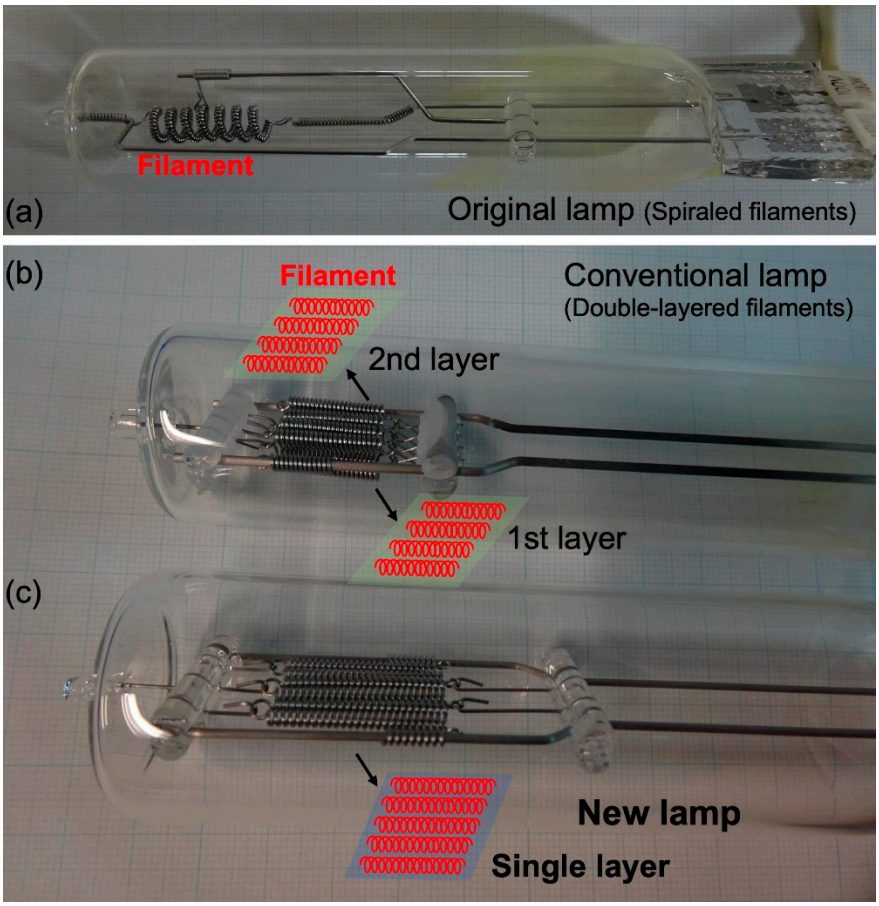

Figure 2. A photograph of (**a**) a halogen lamp with spiral filament, (**b**) a conventional halogen lamp with double-layered filament structure, and (**c**) a new lamp with single-layered filament structure. For clarify, the filament arrays are sketched.

3. Results and Discussion

3.1. Crystal Growth with the Newly Developed Filament

The detailed procedure of the crystal growth including the rod preparation is described in ref. [18]: The feed speed is typically 28–30 mm/h, and the growth speed is 45 mm/h in the gas mixture of O_2 (15%) and Ar (85%) at 0.35 MPa. We note that we prepared two identical feed rods with the same diameter (6 mm) in order to directly compare the growth by the different filaments (double-layer or single-layer). Figure 3a shows a photo of the crystal growth of Sr_2RuO_4 using the conventional filaments with double-layered structure [18]. The molten zone is kept stable with the length of 8 mm, but frequent manual operation was required of the feed speed and power in order to obtain that stability, as has been the case in all image furnace Sr_2RuO_4 growths to date. Figure 3b shows a photo of the growth using the new filament with the single-layered structure. It is obvious that the length of the molten zone is reduced to 5 mm, and the zone is well melted. This suggests that the new filament has the capability to sufficiently melt the feed rod and to form the molten zone in the narrower range. More importantly, the molten zone using the new filament was observed to be far more stable than the conventional one, and consequently, the requirement for manual control was significantly decreased during the entire growth. Finally, the obtained crystal had a length of 12 cm length, compared to the 7 cm typically obtained using the conventional filament, as summarized in Figure 4. We note that the growth was forced to stop at the crystal length of 12 cm only because the lower shaft reached the lower limit set in the furnace, and not due to any zone instability. Thus, it is confirmed that the newly developed filament contributes to the growth of Sr_2RuO_4 under stable conditions. It is also worth describing that, when we start the growth, input power

to the single-layered (double-layered) filament is 1.51 (1.12) kW, respectively. The necessity of higher power for the new filament might be reflected by the following reason: (i) A steeper temperature gradient yields enhanced heat-flow from the zone to the feed/seed. Consequently, it needs more input power to keep the molten zone stable under sufficiently melted condition. (ii) Since the total volume of the new filament was reduced by 40%, more input power is necessary to generate 2000 °C at the molten zone. Although more input power is necessary for the growth of Sr_2RuO_4 with the new filaments, we argue that the required power is still only 80% full available power. On the basis of our acquired experience so far, we are able to estimate that lifetime of the new filament can be 100 times longer than the typical lifetime (200 h) when the filament is continuously used under full power.

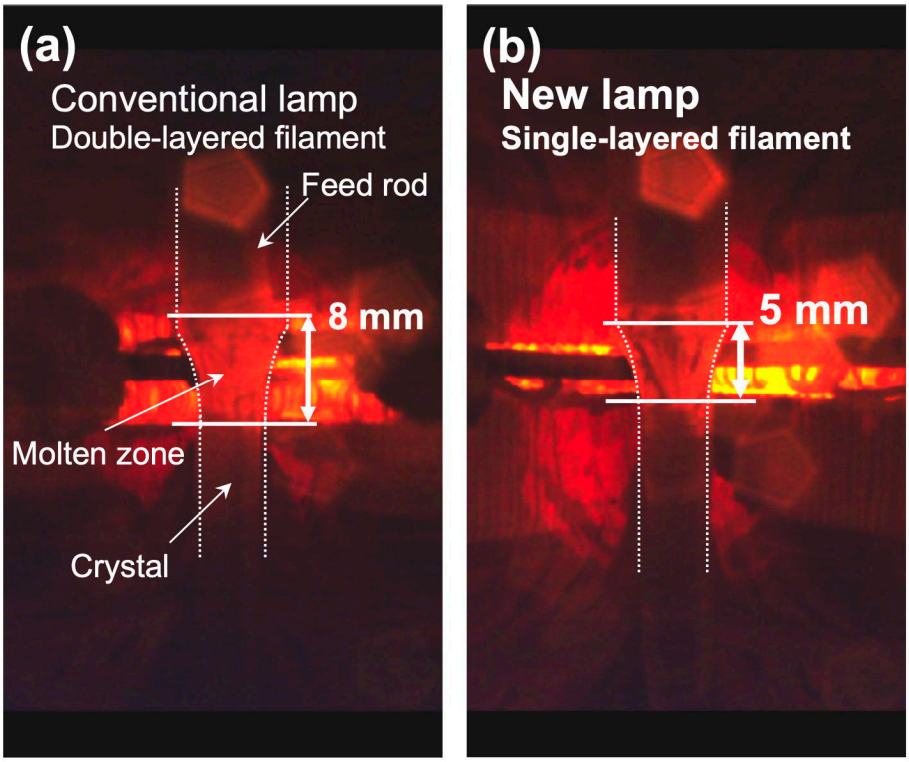

Figure 3. Crystal growth of Sr_2RuO_4 with (**a**) conventional halogen lamps with double-layered filament and (**b**) new lamps with single-layered filament. A narrower molten zone is obtained by using the new lamp. For clarify, dotted lines and curves are added for guides.

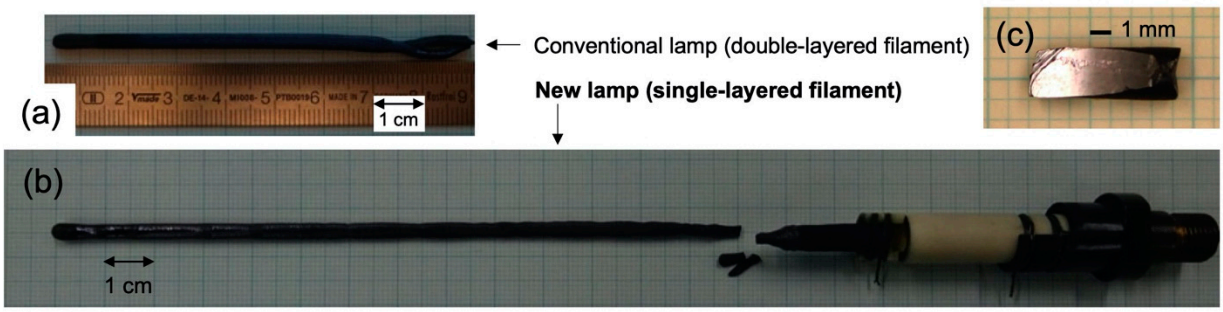

Figure 4. Photograph of the grown crystals using (**a**) conventional halogen lamps with double-layered filament and (**b**) new lamps with single-layered filament. (**c**) A photograph of the cleaved crystal. The shiny surface represents the (001) plane.

3.2. Characterization of the As-Grown Crystal

Figure 5 shows the back-scattered Laue photograph of the crystal grown using the new filament, after the sample was cleaved as seen in Figure 4c. Here, the photograph along the [001] direction in Figure 5 is reversed white and black for clarity. We can see sharp spots, suggesting the high quality. In order to characterize the quality of the grown crystals in more detail, we performed $2\theta/\omega$ and rocking curve measurements on the cleaved surface by using an X-ray SmartLab diffractometer (RIGAKU) equipped with Cu-rotator anode (45 kV, 200 mA, Cu *Ka*). The rocking curve is a measure of mosaic spread in the crystal. Figure 6 shows the $2\theta/\omega$ patterns of the cleaved surface between 5 and 140°. The sharp peaks correspond to the 00*l* reflection. The *c*-axis lattice parameter is obtained as 1.275 nm at room temperature, which is in good agreement with a previous report [1]. The inset of Figure 6 shows the 006 rocking curves for the crystals grown using the new filament (solid curve) and the conventional filament (dashed curve). Here, the peaks are normalized to the same height for easy comparison of the full width at half maximum (FWHM). The FWHM is 0.020° and 0.023°, respectively. These values are comparable to a cuprate $YBa_2Cu_3O_{6.95}$ grown in Y_2O_3 stabilized ZrO_2 crucibles, but the values of Sr_2RuO_4 are still higher than that of the $YBa_2Cu_3O_{6.95}$ crystals (0.007) grown in $BaZrO_3$ crucibles [40]. This result suggests that in terms of mosaic spread, the quality of the grown Sr_2RuO_4 is not particularly sensitive to the difference of the filaments used for the growth.

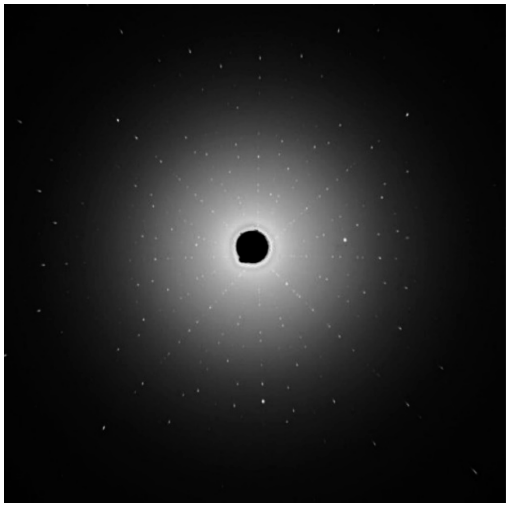

Figure 5. A back-scattered Laue photograph along the [001] axis.

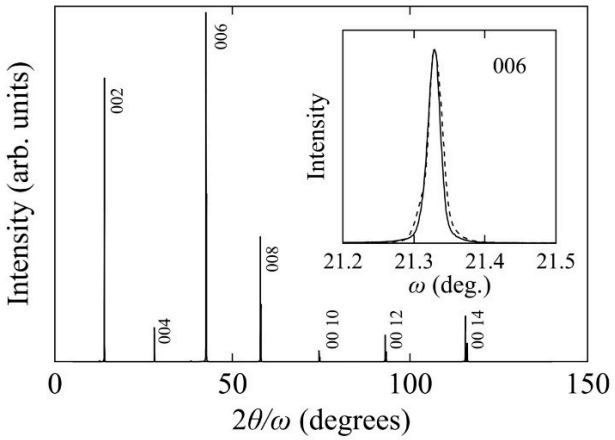

Figure 6. $2\theta/\omega$ scanned XRD pattern of the cleaved surface of Sr_2RuO_4 grown using the new filament. The inset shows the (006) rocking curves for the crystals grown by the new filament (full curve) and the conventional filament (dashed curve).

Another important physical property to be characterized is T_c in bulk, and we measured the temperature (T) dependence of specific heat (C_p) below 2 K using an option of Physical Properties Measurements System (PPMS, Quantum Design) by a relaxation method in order to check the bulk superconductivity. The heat capacity C_p divided by T (C_p/T) as a function of temperature is presented in Figure 7. We can see a clear and sharp superconducting transition at 1.5 K, along with a small residual density of states, which is deduced by extrapolating C_p/T to zero Kelvin. Additionally, the specific-heat jump at T_c ($\Delta C_p/\gamma_N T_c$) is 0.72, where γ_N is the electronic specific heat coefficient in the normal state [41]. These results show that the crystal grown using the new filament is of high quality, at least as good and arguably better than those of crystals obtained by the crystals using the conventional filament [18]. Consequently, the grown crystals in this study can be suitable for further research such as neutron scattering experiments [35] that require very large crystals or using techniques such as resonant ultrasound which requires careful cutting and polishing of samples of well-defined shape from large starting crystals [42,43].

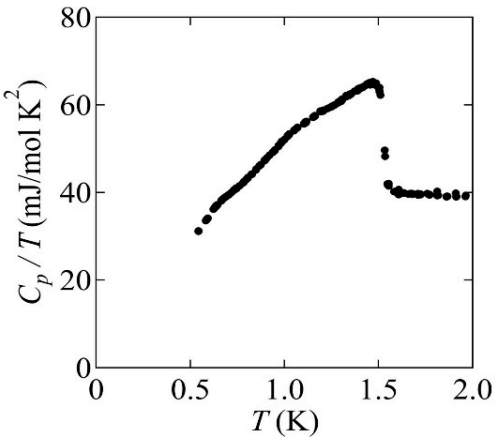

Figure 7. Specific heat divided by temperature (C_P/T) as a function of temperature below 2 K. A clear transition at 1.5 K is seen. Additionally, the residual density of states is small when C_P/T extrapolates to zero Kelvin.

4. Concluding Remarks

We have demonstrated the improvement of the crystal growth of Sr_2RuO_4 using an improved filament with single-layered structure. The new filament has the same maximum power (2 kW) as the conventional double-layered filament. The molten zone is narrower, enabling better stability during growth. We succeeded in obtaining larger crystals fully 12 cm long, the maximum size available for our furnace. X-ray and heat capacity characterization demonstrate that the grown crystal has high quality. We also note that the growth of another ruthenate, $Ca_3Ru_2O_7$, was successful using the new filament. We therefore emphasize the suitability of the new filament for the crystal growth of materials with low viscosity melts and low surface tension.

Another option to narrow the molten zone is to use laser emission, which has seen dramatic developments in recent years [44], and has been reported to have high potential for good molten-zone stability and control [45]. Laser emission can make the zone even narrower than that obtained by the radiation from halogen lamps. However, a "disadvantage" of laser emission can be that the zone is too sharply defined, leading to cracking of the as-grown crystal because of too sharp a temperature gradient between the molten zone and the grown crystal. Therefore, reduction of the temperature gradient has been developed by improving the laser profile [45]. We note that this kind of cracking was not seen in our cleaved crystals, as shown in Figure 4c.

A further advantage of using the new filament is flexibility. We are able to replace the lamps using the same furnaces. Since nearly a thousand of the infrared image furnaces have been installed over the world, replacing the lamps is more practical and reliable compared

to the installation of new laser units. It is also possible to use different lamps for materials with different surface tension/viscosity melts, if appropriate. Although developing the laser-emitted floating-zone technique has high potential to advance the field [46], we show here that the "classical method" still has potential both for improvement and for the extension to the crystal growth of materials with such low surface tension/viscosity melts that it has been impossible, so far, to obtain the crystals by floating zone growth.

Author Contributions: N.K., D.A.S. and A.P.M. planned this project. T.N. developed the halogen lamps with the single-layered filament. N.K. and D.A.S. grew the crystals and characterized them. The manuscript was prepared mainly by N.K. and A.P.M. with the input from all the authors. All authors have read and agreed to the published version of the manuscript.

Funding: This work is supported by a KAKENHI Grants-in-Aids for Scientific Research (Grant Nos. 17H06136, 18K04715, and 21H01033) from the Japan Society for the Promotion of Science (JSPS) and by a JST-Mirai Program (Grant No. JPMJMI18A3).

Institutional Review Board Statement: Not applicable.

Informed Consent Statement: Not applicable.

Data Availability Statement: The data are contained within the article.

Acknowledgments: We acknowledge C.W. Hicks for the useful comments and discussion, Yoshiteru Maeno for valuable information about the development ruthenate growth techniques during the 1990s, Takanobu Hiroto for technical support for the rocking curve and $2\theta/\omega$ measurements, and Hideo Mishina for useful information.

Conflicts of Interest: T.N. is an employee of Canon Machinery Inc. in Japan.

References

1. Maeno, Y.; Hashimoto, H.; Yoshida, K.; Nishizaki, S.; Fujita, T.; Bednorz, J.G.; Lichtenberg, F. Superconductivity in a layered perovskite without copper. *Nature* **1994**, *372*, 532. [CrossRef]
2. Mackenzie, A.P.; Maeno, Y. The superconductivity of Sr_2RuO_4 and the physics of spin-triplet pairing. *Rev. Mod. Phys.* **2003**, *75*, 657. [CrossRef]
3. Maeno, Y.; Kittaka, S.; Nomura, T.; Yonezawa, S.; Ishida, K. Evaluation of Spin-Triplet Superconductivity in Sr_2RuO_4. *J. Phys. Soc. Jpn.* **2012**, *81*, 011009. [CrossRef]
4. Mackenzie, A.P.; Scaffidi, T.; Hicks, C.W.; Maeno, Y. Even odder after twenty-three years: The superconducting order parameter puzzle of Sr_2RuO_4. *NPJ Quantum Mater.* **2017**, *2*, 40. [CrossRef]
5. Mackenzie, A.P.; Julian, S.R.; Diver, A.J.; McMullan, G.J.; Ray, M.P.; Lonzarich, G.G.; Maeno, Y.; Nishizaki, S.; Fujita, T. Quantum oscillations in the layered perovskite superconductor Sr_2RuO_4. *Phys. Rev. Lett.* **1996**, *76*, 3786. [CrossRef]
6. Bergemann, C.; Mackenzie, A.P.; Julian, S.R.; Forsythe, D.; Ohmichi, E. Quasi-two-dimensional Fermi liquid properties of the unconventional superconductor Sr_2RuO_4. *Adv. Phys.* **2003**, *52*, 639–725. [CrossRef]
7. Damascelli, A.; Lu, D.H.; Shen, K.M.; Armitage, N.P.; Ronning, F.; Feng, D.L.; Kim, C.; Shen, Z.-X.; Kimura, T.; Tokura, Y.; et al. Fermi surface, surface states, and surface reconstruction in Sr_2RuO_4. *Phys. Rev. Lett.* **2000**, *85*, 5194. [CrossRef] [PubMed]
8. Tamai, A.; Zingl, M.; Rozbicki, E.; Cappelli, E.; Riccò, S.; de la Torre, A.; McKeown Walker, S.; Bruno, F.Y.; King, P.D.C.; Meevasana, W.; et al. High-Resolution Photoemission on Sr_2RuO_4 Reveals Correlation-Enhanced Effective Spin-Orbit Coupling and Dominantly Local Self-Energies. *Phys. Rev. X* **2019**, *9*, 021048. [CrossRef]
9. Suderow, H.; Crespo, V.; Guillamon, I.; Vieira, S.; Servant, F.; Lejay, P.; Brison, J.P.; Flouquet, J. A nodeless superconducting gap in Sr_2RuO_4 from tunneling spectroscopy. *New J. Phys.* **2009**, *11*, 093004. [CrossRef]
10. Hassinger, E.; Bourgeois-Hope, P.; Taniguchi, H.; de Cotret, S.R.; Grissonnanche, G.; Anwar, M.S.; Maeno, Y.; Doiron-Leyraud, N.; Taillefer, L. Vertical line nodes in the superconducting gap structure of Sr_2RuO_4. *Phys. Rev. X* **2017**, *7*, 011032. [CrossRef]
11. Kittaka, S.; Nakamura, S.; Sakakibara, T.; Kikugawa, N.; Terashima, T.; Uji, S.; Sokolov, D.A.; Mackenzie, A.P.; Irie, K.; Tsutsumi, Y.; et al. Searching for gap zeros in Sr_2RuO_4 via field-angle-dependent specific-heat measurement. *J. Phys. Soc. Jpn.* **2018**, *87*, 093703. [CrossRef]
12. Sharma, R.; Edkins, S.D.; Wang, Z.; Kostin, A.; Sow, C.; Maeno, Y.; Mackenzie, A.P.; Davis, J.C.S.; Madhavan, V. Momentum-resolved superconducting energy gaps of Sr_2RuO_4 from quasiparticle interference imaging. *Proc. Natl. Acad. Sci. USA* **2020**, *117*, 5222–5227. [CrossRef]
13. Mackenzie, A.P.; Haselwimmer, R.K.W.; Tyler, A.W.; Lonzarich, G.G.; Mori, Y.; Nishizaki, S.; Maeno, Y. Extremely strong dependence of superconductivity on disorder in Sr_2RuO_4. *Phys. Rev. Lett.* **1998**, *80*, 161. [CrossRef]
14. Mao, Z.Q.; Mori, Y.; Maeno, Y. Suppression of superconductivity in Sr_2RuO_4 caused by defects. *Phys. Rev. B* **1999**, *60*, 610. [CrossRef]

15. Kikugawa, N.; Maeno, Y. Non-Fermi-liquid behavior in Sr_2RuO_4 with nonmagnetic impurities. *Phys. Rev. Lett.* **2002**, *89*, 117001. [CrossRef]
16. Kikugawa, N.; Mackenzie, A.P.; Maeno, Y. Effects of In-Plane Impurity Substitution in Sr_2RuO_4. *J. Phys. Soc. Jpn.* **2003**, *72*, 237–240. [CrossRef]
17. Mao, Z.Q.; Maeno, Y.; Fukazawa, H. Crystal growth of Sr_2RuO_4. *Mater. Res. Bull.* **2000**, *35*, 1813. [CrossRef]
18. Bobowski, J.S.; Kikugawa, N.; Miyoshi, T.; Suwa, H.; Xu, H.-S.; Yonezawa, S.; Sokolov, D.A.; Mackenzie, A.P.; Maeno, Y. Improved Single-Crystal Growth of Sr_2RuO_4. *Condens. Matter* **2019**, *4*, 6. [CrossRef]
19. Hicks, C.W.; Brodsky, D.O.; Yelland, E.A.; Gibbs, A.S.; Bruin, J.A.N.; Barber, M.E.; Edkins, S.D.; Nishimura, K.; Yonezawa, S.; Maeno, Y.; et al. Strong Increase of T_c of Sr_2RuO_4 Under Both Tensile and Compressive Strain. *Science* **2014**, *344*, 283–285. [CrossRef]
20. Hicks, C.W.; Barber, M.E.; Edkins, S.D.; Brodsky, D.O.; Mackenzie, A.P. Piezoelectric-based apparatus for strain tuning. *Rev. Sci. Instrum.* **2014**, *85*, 065003. [CrossRef]
21. Barber, M.E.; Lechermann, F.; Streltsov, S.V.; Skornyakov, S.L.; Ghosh, S.; Ramshaw, B.J.; Kikugawa, N.; Sokolov, D.A.; Mackenzie, A.P.; Hicks, C.W.; et al. Role of correlations in determining the Van Hove strain in Sr_2RuO_4. *Phys. Rev. B* **2019**, *100*, 245139. [CrossRef]
22. Steppke, A.; Zhao, L.; Barber, M.E.; Scaffidi, T.; Jerzembeck, F.; Rosner, H.; Gibbs, A.S.; Maeno, Y.; Simon, S.H.; Mackenzie, A.P.; et al. Strong peak in T_c of Sr_2RuO_4 under uniaxial pressure. *Science* **2017**, *355*, eaaf9398. [CrossRef]
23. Barber, M.E.; Gibbs, A.S.; Maeno, Y.; Mackenzie, A.P.; Hicks, C.W. Resistivity in the vicinity of a van Hove singularity: Sr_2RuO_4 under uniaxial pressure. *Phys. Rev. Lett.* **2018**, *120*, 076602. [CrossRef] [PubMed]
24. Li, Y.-S.; Kikugawa, N.; Sokolov, D.A.; Jerzembeck, F.; Gibbs, A.S.; Maeno, Y.; Hicks, C.W.; Nicklas, M.; Mackenzie, A.P. High sensitivity heat capacity measurements on Sr_2RuO_4 under uniaxial pressure. *Proc. Nat. Acad. Sci. USA* **2021**, *118*, e2020492118. [CrossRef] [PubMed]
25. Sunko, V.; Abarca Morales, E.; Marković, I.; Barber, M.E.; Milosavljević, D.; Mazzola, F.; Sokolov, D.A.; Kikugawa, N.; Cacho, C.; Dudin, P.; et al. Direct observation of a uniaxial stress-driven Lifshitz transition in Sr_2RuO_4. *NPJ Quantum Mater.* **2019**, *4*, 46. [CrossRef]
26. Pustogow, A.; Luo, Y.; Chronister, A.; Su, Y.-S.; Sokolov, D.A.; Jerzembeck, F.; Mackenzie, A.P.; Hicks, C.W.; Kikugawa, N.; Raghu, S.; et al. Constraints on the superconducting order parameter in Sr_2RuO_4 from oxygen-17 nuclear magnetic resonance. *Nature* **2019**, *574*, 72–75. [CrossRef]
27. Ishida, K.; Manago, M.; Kinjo, K.; Maeno, Y. Reduction of the ^{17}O Knight Shift in the Superconducting State and the Heat-up Effect by NMR Pulses on Sr_2RuO_4. *J. Phys. Soc. Jpn.* **2020**, *89*, 034712. [CrossRef]
28. Ishida, K.; Mukuda, H.; Kitaoka, Y.; Asayama, K.; Mao, Z.Q.; Mori, Y.; Maeno, Y. Spin-triplet superconductivity in Sr_2RuO_4 identified by ^{17}O Knight shift. *Nature* **1998**, *396*, 658–660. [CrossRef]
29. Grinenko, V.; Ghosh, S.; Sarkar, R.; Orain, J.-C.; Nikitin, A.; Elender, M.; Das, D.; Guguchia, Z.; Brückner, F.; Barber, M.E.; et al. Split superconducting and time-reversal symmetry-breaking transitions, and magnetic order in Sr_2RuO_4 under uniaxial stress. *Nat. Phys.* **2021**. [CrossRef]
30. Liu, Y.-C.; Zhang, F.-C.; Rice, T.M.; Wang, Q.-H. Theory of the evolution of superconductivity in Sr_2RuO_4 under anisotropic strain. *NPJ Quantum Mater.* **2017**, *2*, 1. [CrossRef]
31. Suh, H.G.; Menke, H.; Brydon, P.M.R.; Timm, C.; Ramires, A.; Agterberg, D.F. Stabilizing even-parity chiral superconductivity in Sr_2RuO_4. *Phys. Rev. Res.* **2020**, *2*, 032023. [CrossRef]
32. Yonezawa, S.; Kajikawa, T.; Maeno, Y. First-order superconducting transition of Sr_2RuO_4. *Phys. Rev. Lett.* **2013**, *110*, 077003. [CrossRef] [PubMed]
33. Kittaka, S.; Kasahara, A.; Sakakibara, T.; Shibata, D.; Yonezawa, S.; Maeno, Y.; Tenya, K.; Machida, K. Sharp magnetization jump at the first-order superconducting transition in Sr_2RuO_4. *Phys. Rev. B* **2014**, *90*, 220502. [CrossRef]
34. Kikugawa, N.; Terashima, T.; Uji, S.; Sugii, K.; Maeno, Y.; Graf, D.; Baumbach, R.; Brooks, J. Superconducting subphase in the layered perovskite ruthenate Sr_2RuO_4 in a parallel magnetic field. *Phys. Rev. B* **2016**, *93*, 184513. [CrossRef]
35. Ghosh, S.; Brückner, F.; Nikitin, A.; Grinenko, V.; Elender, M.; Mackenzie, A.P.; Luetkens, H.; Klauss, H.-H.; Hicks, C.W. Piezoelectric-driven uniaxial pressure cell for muon spin relaxation and neutron scattering experiments. *Rev. Sci. Instrum.* **2020**, *91*, 103902. [CrossRef]
36. Ikeda, S.I.; Azuma, U.; Shirakawa, N.; Nishihara, Y.; Maeno, Y. Bulk single-crystal growth of strontium ruthenates by a floating-zone method. *J. Cryst. Growth* **2002**, *237–239*, 787–791. [CrossRef]
37. Perry, R.S.; Maeno, Y. Systematic approach to the growth of high-quality single crystals of $Sr_3Ru_2O_7$. *J. Cryst. Growth* **2004**, *271*, 134–141. [CrossRef]
38. Kikugawa, N.; Balicas, L.; Mackenzie, A.P. Physical Properties of Single-Crystalline $CaRuO_3$ Grown by a Floating-Zone Method. *J. Phys. Soc. Jpn.* **2009**, *78*, 014701. [CrossRef]
39. Kikugawa, N.; Baumbach, R.; Brooks, J.S.; Terashima, T.; Uji, S.; Maeno, Y. Single-Crystal Growth of a Perovskite Ruthenate $SrRuO_3$ by the Floating-Zone Method. *Cryst. Growth Des.* **2015**, *15*, 5573. [CrossRef]
40. Liang, R.; Bonn, D.A.; Hardy, W.N. Growth of high quality YBCO single crystals using $BaZrO_3$ crucibles. *Phys. C Supercond.* **1998**, *304*, 105–111. [CrossRef]

41. NishiZaki, S.; Maeno, Y.; Mao, Z. Effect of impurities on the specific heat of the spin-triplet superconductor Sr_2RuO_4. *J. Low Temp. Phys.* **1999**, *117*, 1581–1585. [CrossRef]
42. Benhabib, S.; Lupien, C.; Paul, I.; Berges, L.; Dion, M.; Nardone, M.; Zitouni, A.; Mao, Z.Q.; Maeno, Y.; Georges, A.; et al. Ultrasound evidence for a two-component superconducting order parameter in Sr_2RuO_4. *Nat. Phys.* **2021**, *17*, 194–198. [CrossRef]
43. Ghosh, S.; Shekhter, A.; Jerzembeck, F.; Kikugawa, N.; Sokolov, D.A.; Brando, M.; Mackenzie, A.P.; Hicks, C.W.; Ramshaw, B.J. Thermodynamic evidence for a two-component superconducting order parameter in Sr_2RuO_4. *Nat. Phys.* **2021**, *17*, 199–204. [CrossRef]
44. Ito, T.; Ushiyama, T.; Yanagisawa, Y.; Tomioka, Y.; Shindo, I.; Yanase, A. Laser-diode-heated floating zone (LDFZ) method appropriate to crystal growth of incongruently melting materials. *J. Cryst. Growth* **2013**, *363*, 264–269. [CrossRef]
45. Kaneko, Y.; Tokura, Y. Floating zone furnace equipped with a high power laser of 1 kW composed of five smart beams. *J. Cryst. Growth* **2020**, *533*, 125435. [CrossRef]
46. Rey-García, F.; Ibáñez, R.; Angurel, L.A.; Costa, F.M.; de la Fuente, G.F. Laser Floating Zone Growth: Overview, Singular Materials, Broad Applications, and Future Perspectives. *Crystals* **2021**, *11*, 38. [CrossRef]